





Cite this: DOI: 10.1039/d4nr05442c

## Optically active chiral photonic crystals exhibiting enhanced fluorescence and circularly polarized luminescence†

Qilin Guo, Xingye Huang, Huateng Li, Jia Guo  and Changchun Wang \*

Photonic crystals with advanced, unique and well-defined functional nanostructures demonstrate exquisite controllable modulation in light harvesting and emission for unrivalled optical performance. Herein, through ingeniously integrating aggregation-induced emission (AIE) luminogens and chiral helical media into ordered periodic structures, the resulting optically active photonic crystal films exhibit an enhanced photoluminescence (PL) characteristic (increased to 2.2 times the original value) and distinctive emerging circular dichroism (CD) responses near the photonic bandgap (PBG) of the photonic crystal. The modulation of the PL intensity and CD signal peak position is precisely achieved by regulating the PBG by facily tuning the size of the colloidal nanoparticles. Such an interesting phenomenon is mainly the consequence of the PBG edge enhancement effect (including the slow photon effect) and bandgap separation arising from chirality. Remarkably, the boosted fluorescence facilitates the synergistic effect of valid chirality transfer among achiral AIEgens and chiroptical media in a photonic matrix, which effectively contributes to the enhanced circularly polarized luminescence (CPL) activity, thereby expanding the potential applications of CPL-based optically active photonic materials in circularly polarizing emitting devices.

Received 26th December 2024,  
Accepted 26th February 2025

DOI: 10.1039/d4nr05442c

rsc.li/nanoscale

## Introduction

Natural creatures with a hierarchical complex and sophisticated macro-/nano-structure at multiple length scales exhibit tremendous manipulability of exceptional photonic characteristics, enabling effective light propagation and harvesting for a variety of optimized optical multifunctional applications, including vision detection, information storage, photosynthesis, and signal transduction.<sup>1–10</sup> A striking example is the wing of Morpho butterflies, which features brilliant blue structural color due to the constructive interference of multilayer reflected light from the unique and well-defined periodic lamellar structure that is formed by densely arranged nanoscale ridges.<sup>11,12</sup> Besides, the elytron of beetles consists of chiral and cuticular ordered periodic photonic nanostructures with helicoidal orientation, contributing to their exceptional ability to selectively filter left circularly polarized light.<sup>13</sup> Inspired by these natural designs, a diverse range of progressing artificial photonic materials with naturally engineered

structures have been developed, promising novel next-generation smart optical devices for desirable and sustainable practical applications.<sup>14–21</sup>

Photonic crystals (PCs), a class of structurally colored materials, feature highly multiscale, well-ordered periodic dielectric architectures that are comparable to the wavelengths of visible light. These structures are created using distinct components with varying refractive indices, which induce specific photonic bandgaps (PBGs) that manipulate the orientation of light propagation within the crystal lattice, resulting in iridescent reflections.<sup>22–31</sup> In particular, the photonic bandgap allows light to exist as a standing wave mode that resonates with the photonic lattice, in which light travels with a group velocity approaching zero at wavelengths corresponding to the edges of these stopbands.<sup>32–36</sup> This phenomenon is referred to as “slow photons”.<sup>37</sup> Therefore, when incorporating various luminescent materials such as organic molecules or luminogens with an aggregation-induced emission (AIE) character (AIEgens) into photonic crystals, the developed light-matter interactions are significantly enhanced, thus improving absorption and emission properties.<sup>38–44</sup> In addition, chiral helical copolymers with intrinsic handedness have been introduced into a photonic crystal medium to explore the unique capability of the PBG in modulating the light polarization mode, endowing composite photonic crystal materials with distinctive optical activity.<sup>45,46</sup> Furthermore, it is well known

State Key Laboratory of Molecular Engineering of Polymers, Department of Macromolecular Science and Laboratory of Advanced Materials, Fudan University, Shanghai 200433, China. E-mail: ccwang@fudan.edu.cn

† Electronic supplementary information (ESI) available: Experimental materials and characterization methods, details on nanoparticles. See DOI: <https://doi.org/10.1039/d4nr05442c>



that the bonding assembly of luminescent substances with chiral media tends to induce an incredibly effective chirality transfer, which results in luminescent systems emitting left- and right-handed circularly polarized light (LCP/RCP) with different emission intensities, in turn producing circularly polarized luminescence (CPL).<sup>47–55</sup> Consequently, integrating chiral helical media and fluorescent emitters within photonic crystals is expected to yield intriguing optical properties, including fluorescence enhancement, modulation of chiral signals, and the generation of circularly polarized luminescence. These advancements present considerable and promising prospects for optically active photonic crystal materials in potential applications, such as three-dimensional optical displays,<sup>56</sup> asymmetric syntheses and catalysis,<sup>57</sup> optoelectronic devices<sup>58</sup> or circularly polarizing beamsplitter.<sup>59</sup>

In this work, we demonstrate the constructive fabrication of optically active photonic crystal materials with typical CPL performance based on effective chirality transfer in a photonic matrix comprising AIE units and chiral helical copolymers. The PBG edge enhancement effect and slow photon effect of PCs contribute to the remarkably enhanced photoluminescence (PL) property of the tetraphene (TPE) element in the confined rigid cross-linked polymer network, in which the restriction of intramolecular motions (RIM) is intensely manipulated to inhibit the non-radiative decay pathway of excitons and promote the radiative channels. What is more, the composite photonic films exhibit emerging circular dichroism (CD) responses with mirror-image CD signals approaching the PBG of PCs attributed to the bandgap separation in the chiral photonic structures. Owing to the efficient chiral-transfer process between the AIE character and chiral helical copolymers, the emission efficiency of the system is improved for displaying the enhanced CPL activity, providing remarkable tunability and robustness in promisingly the creation of CPL-based photonic crystal materials.

## Results and discussion

Learned from nature, there are various sophisticated optical and structural designs for exceptional photonic functions in different luminescent organisms. For instance, the fireflies wondrously display intense CPL effects (see Fig. 1a) owing to the light polarization that arises from the composited interaction between periodic cuticle layer stacking and chiral medium.<sup>60</sup> To create such multi-functional photonic luminescent material, a novel biomimetic optically active photonic crystal is established (Fig. 1b). During our design, core/shell colloidal nanoparticles are employed for the fabrication of well-ordered periodic photonic structures. AIEgens and chiral helical copolymers in the photonic matrix are conducted to produce effective chirality transfer to endow photonic materials with optical activity. Initially, four kinds of monodisperse PS@P(EA-co-AA) core/shell nanoparticles with various diameters ranging from 145 to 204 nm were fabricated by semi-continuous emulsion polymerization. The related charac-

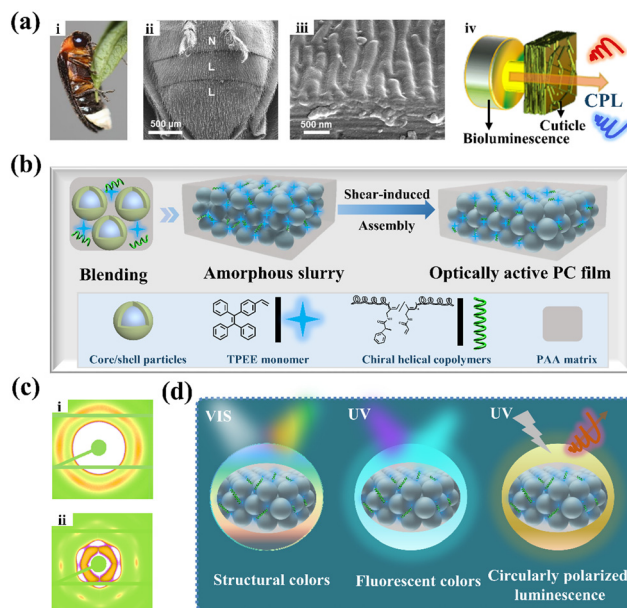


**Fig. 1** Biomimetic optically active photonic crystal design. (a) Illustrative image of a firefly light organ: (i) optical image of a firefly (*L. lateralis* Motschulsky) in males; (ii) surface and (iii) cross-sectional SEM images of the abdominal segments of a firefly, including normal (N) and lantern (L) cuticles; and (iv) schematic diagram of the bioluminescence emitted from firefly lanterns passing through the ordered cuticle to convert it into circularly polarized light. Adapted with permission.<sup>60</sup> Copyright 2012, National Academy of Sciences. (b) Schematic illustration of the shear-induced assembly for preparing composite photonic crystal films. (c) 2D USAXS patterns of (i) particle slurry and (ii) photonic films. (d) Schematic of the PC films enabling multilevel optical performance.

terization information of the as-prepared nanoparticles is shown in the ESI.† The growth of particle diameters at each step of polymerization was obtained from the TEM images shown in Fig. S1.† In addition, the size distribution histogram of the PS core based on TEM analysis further demonstrates the great monodispersity of uniform colloidal nanoparticles (Fig. S2†), which is a prerequisite for constructing long-range ordered structures as physical blocking units. Afterwards, the chiral helical copolymer poly(*N*-propargyl acrylamide)-random-poly(*N*-propargyl-(*R/S*)-phenylpropanoamide) (PM1-*r*-PM2) was synthesized through a solution copolymerization reaction in the presence of a rhodium catalyst (Fig. S3–S6†).<sup>61</sup> The obtained chiral copolymers could be further photopolymerized with other vinyl-containing monomers such as (2-(4-vinylphenyl)ethene-1,1,2-triyl)tribenzene (TPEE) or polymer matrix (AA) of photonic crystals for constructing stable and functional optically active photonic films. Owing to the superior features of the molecule-mediated shear-induced assembly technique (MSAT),<sup>62</sup> multiple building units can be perfectly integrated without affecting the ordered arrangement of colloids, thus forming homogeneous structural color materials. As illustrated in Fig. 1c, 2D ultrasmall-angle X-ray scattering (USAXS) was employed to further verify the evolution of the arrayed structure before and after shear-induced ordering assembly. The



apparent diffraction spots were observed in the composite photonic films, indicating typical long-range ordered periodic structures, while no clear spots were present in the blending slurry. Finally, this distinct scheme results in an expected composite optically active photonic crystal film, which comprises tunable structural color, chirality and enhanced fluorescence property, even featuring active CPL response (Fig. 1d).

To investigate in more detail the impact of individual components on the composite optically active photonic crystal films, fluorescence performance was first explored, as illustrated in Fig. 2. Owing to the powerful tool of MSAT, the tailoring of monodispersed colloidal nanoparticles enables precise arrangement engineering for generating well-ordered periodic

nanostructures. Consequently, highly saturated colored photonic films with gradual change from blue to red were obtained through the shearing assembly of colloidal particles with varied diameters (Fig. 2a), which is evidenced by the fact that four representative single peaks with reflection maximum varied at 456, 508, 565 and 607 nm for blue, green, yellow and red, respectively (Fig. 2b). Additionally, the surface structure characterization further confirmed the formation of closely packing long-range ordered arrays utilized by Scanning Electron Microscopy (SEM), which is also verified by the apparent sharp diffraction spot patterns in 2D fast Fourier-transform (FFT) diagrams (Fig. S7†). Such a periodic photonic structure can create coherent light scattering to yield sparkling structural colors, which is consistent with their optical appearance under white light (Fig. 2a). As expected, a brilliant blue fluorescent emission with a maximum wavelength of around 495 nm at an excitation wavelength of 370 nm was observed in the composite photonic films because the TPE molecules were embedded in the photonic crystal matrix (Fig. 2c and d). It is widely known that TPE monomers, as a kind of AIEgen, can induce effective fluorescence emission by the aggregate formation with AIE property.<sup>63,64</sup> When incorporating these TPE units into the photonic crystal matrix, the confined rigid polymer network possesses a more efficient restriction of intramolecular motions (RIMs) of AIEgens,<sup>65</sup> producing typically vivid blue fluorescent color (Fig. 2c). Besides, the collected reflection spectrum creates more clarity on the distinctive dual optical state in the CIE diagrams under white light or UV irradiation (Fig. 2e and f).

Interestingly, the composite photonic crystal films exhibit great fluorescence enhancement compared to neat AIE films with the same TPE concentration, as shown in Fig. 2d and S8.† We attribute this phenomenon to two factors: the photonic bandgap edge enhancement effect and the slow photon effect of the photonic crystal. Owing to the overlapping of fluorescence emission wavelength with the PBG edge of colored films, the fluorescence can be amplified.<sup>36</sup> Pronouncedly, the green film displays the highest boosted fluorescence intensity (increased to 2.2 folds) owing to the emission peak position of the TPE, which matches well with the PBG edge of the green PC film, exhibiting intense fluorescence coupling. Notably, prior to exhaustively exploring the impact of PBG on AIE fluorescence emission intensity, the thicknesses of different composite photonic films were excluded to avoid potential external influences (Fig. S9†).

Another two composite photonic films with quasi-ordered and amorphous structures were employed to affirm that the fluorescence enhancement is mainly contributed by the PBG edge effect. The photonic glass (PG) film with short-range ordered arrays and a similar green reflected color was observed, as indicated by the SEM image, digital picture and reflection wavelength in Fig. S10a and S10b.† Although PG films can trigger the pseudo PBG matching the emission wavelength of AIEgens to effectively boost the PL intensity, the degree of enhancement is relatively weak compared with that of photonic crystals (Fig. S10e†). This suggests that only the

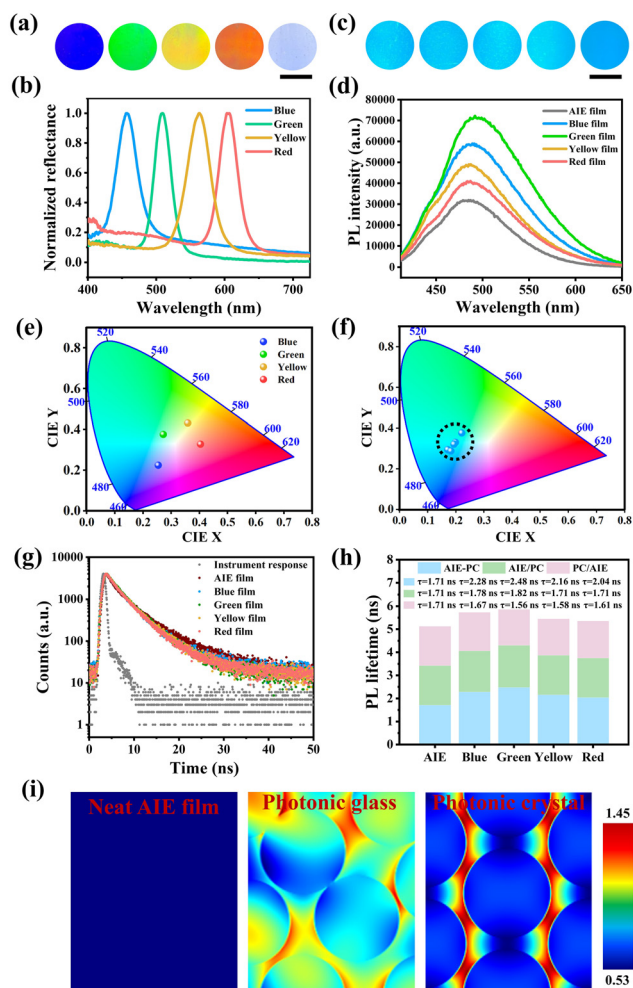


**Fig. 2** Enhanced fluorescence emission properties of the composite photonic crystals. (a) Photographs, (b) reflection spectra and (e) CIE diagrams of the photonic films with tunable colors. (c) Photographs, (d) photoluminescence (PL) spectra and (f) CIE diagrams of the photonic films under UV irradiation ( $\lambda = 370$  nm). Panels (a) and (c) show blue, green, yellow, red and AIE films (from left to right). The scale bar is 1 cm. (g) Time-resolved single-photon counting data of the composite photonic films. (h) Summarized lifetimes of the composite photonic films. (i) Simulated electric field distributions for the neat AIE, photonic glass and photonic crystal AIE films.



true photonic bandgap in the photonic crystal could maximize enhanced fluorescence emission. For amorphous films, no structural color was obtained owing to the disordered nanostructures for multiple incoherent scattering, as confirmed *via* the reflection spectrum and SEM image (Fig. S10c and S10d<sup>†</sup>), that is, no effective PBG appears in the amorphous film. Eventually, the PL intensity of amorphous film remains almost constant with pure AIE film (Fig. S10e<sup>†</sup>). All these results indicate that the existence of the PBG effect can significantly enhance fluorescence emission, which provides an effective platform to facilitate the introduction of photonic crystals, thus endowing AIEgens with high luminescence and facilitating the enormous optical applications of active PL-enhanced photonic crystal materials.

Subsequently, we focus on attempting to elucidate the PL enhancement mechanism from the perspective of the “slow photons” effect, which could contribute to a reduced group velocity of light propagation for strongly improving the relaxation processes.<sup>33,37</sup> The TPE lifetimes of different films were examined by the time-correlated single-photon counting. As illustrated in Fig. 2g, the exciton lifetimes were 1.71 ns for neat AIE film, 2.28 ns for blue film, 2.48 ns for green film, 2.16 ns for yellow film and 2.04 ns for red film. According to the expression of the intensity of excited state fluorescent molecules decaying:  $I_t = I_0 \exp(-t/\tau)$ , where  $I_0$  represents the initial PL intensity,  $I_t$  represents the intensity detected at a certain time, and  $\tau$  represents the fluorescence lifetime. Thus, the significant increase in PL lifetime leads to the corresponding enhanced PL intensity because other factors remain almost constant in different photonic films. This indicates that the intramolecular rotations of the TPE monomer embedded in the photonic crystal matrix are intensely restricted owing to the involved physical polymer network constraint, which greatly strengthens the radiative relaxation of excited states while blocking the non-radiative decay channel.

To further clarify that it is the intrinsic slow photon effect of the PC film that improves the PL emission, neat photonic films were placed on top of or beneath the pure AIE film to demonstrate the regulation of fluorescence intensity at varied positions. As shown in Fig. S11a and 11b,<sup>†</sup> when the PC film was placed beneath the neat AIE film (AIE/PC), the improved PL emission was observed owing to the enhancement of the 3D PC surface effect on fluorescent molecules.<sup>66</sup> However, the modulation of PL intensity is slightly inferior to that of the composite AIE PC film (AIE-PC). What is more, when the PC film was placed above the AIE film (PC/AIE), obvious inhibition of PL intensity occurred (Fig. S11c and 11d<sup>†</sup>), which is derived from the reflected dissipation of light by photonic crystals reducing the luminescence efficiency of fluorescent monomers. The corresponding lifetime is illustrated in Fig. 2h, Fig. S11e and S11f,<sup>†</sup> which further demonstrates the “slow photon” effect only existing inside photonic crystals, thus increasing the interaction between photons and AIEgens to improve radiation efficiency. Moreover, the fluorescence lifetimes of TPE in PG films (2.38 ns) and amorphous films (1.77

ns) were measured, as depicted in Fig. S10f,<sup>†</sup> clearly indicating that the improved fluorescence emission is mainly responsible for the selective enhancement at the bandgap edge of the true PBG in the photonic crystal owing to the slow photon effect. What is more, finite-difference time-domain (FDTD) simulation was used to further analyse the electric field distributions of neat AIE film, composite AIE-PG film and AIE-PC film to demonstrate the fluorescence enhancement effect. As shown in Fig. 2i, the uniform electric field distributes on the whole AIE film, implying no increased fluorescence emission in the homogenous neat AIE system. However, the introduction of a short-range ordered structure for photonic glass contributes to the apparent near-field enhancement located in the mixing matrix domains, and the maximum value of the near-field enhancement reaches the greatest value in the photonic crystal with long-range ordered arrays. Generally, the local electric field intensity distribution of photonic crystals has been confirmed to be a positive function of fluorescence intensity.<sup>67</sup> In this case, the raised electric field intensity distribution dictates that the periodic structure of photonic crystals has a promoting effect on enhancing AIE fluorescence emission.

Circular dichroism and UV-vis absorption spectroscopies were employed to fully characterize the chiral properties of composite photonic crystal films. For neat AIE film, the intense mirror-image CD signals with an opposite sign of around 375 nm originating from chiral helical polymer chains were measured, in which the plus Cotton effect depends on the AIE film with *R*-copolymers, while the minus Cotton effect is found in the presence of AIE film with *S*-copolymers (Fig. 3a). Excitingly, composite PC films are provided with inherent chiral signs derived from chiral polymers, and new CD response signals are also depicted near the PBG of photonic crystals (Fig. 3b–e). In addition, UV-vis absorption spectra were used to evaluate the respective peak positions of chiral

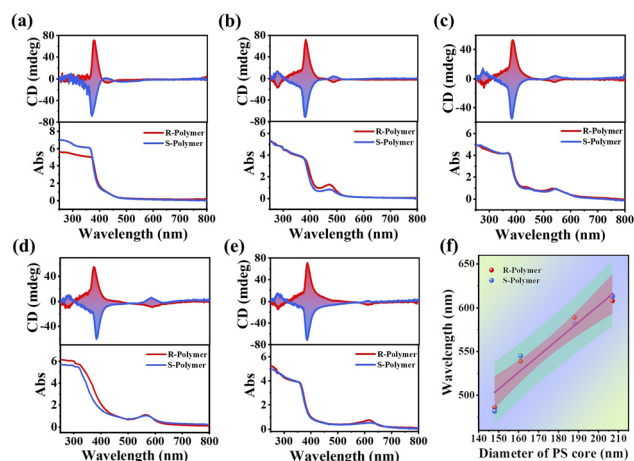


**Fig. 3** Optically active chiral properties of the composite photonic crystals. CD and UV-vis absorption spectra of (a) the neat AIE film and (b) blue, (c) green, (d) yellow and (e) red composite photonic films. (f) Emerging CD signals as a function of colloidal nanoparticle diameters.



copolymers and photonic crystals (Fig. 3b–e). What is more, the tailored CD signals can be readily tuned by simply controlling the variety of relative PBG of the photonic crystal films, in which the resultant CD signal peaks nearly scale linearly with the diameter of colloidal nanoparticles (Fig. 3f). We suggest that the simultaneous presence of photonic bandgaps and chiral media gives rise to this phenomenon and is attributed to the new CD signal peaks generated to the band gap separation in photonic crystals composed of chiral helical polymer medium.<sup>46,68,69</sup> For pure PC films without chiral media, no specific polarization state of light (multiple states or overlapping situations) emerges through the homogeneous PC owing to the left-hand/right-hand circularly polarized light possessing the same bandgap structure. This implies that the optical mode exhibited by the photonic crystal film in this situation is degenerate. Consequently, neat PC films perform silent CD signals, as shown in Fig. S12a.† However, the introduction of chiral copolymers into the PC matrix contributes to LCP and RCP with different bandgap structures stemming from the existence of varied refraction indexes in mixture media, which greatly makes the polarization of light uniquely determined and displays a nondegenerate state for new CD signals close to the PBG of PC. The reported results, such as FDTD simulation, further confirmed that introducing chirality into PCs may break the degeneracy, resulting in the spectra for LCP and RCP light being separated in opposite directions, with changes in both the bandgap widths and the positions of the defect modes.<sup>69</sup> Additionally, the composite PG film with pseudo PBG and amorphous film with no PBG reveals that the emerging CD signals are almost zero value except for the inherent optical activity of chiral copolymers (Fig. S12b and c†), which discloses the critical role of PBG of the photonic crystal in inducing the emerging CD responses. It turns out that only the presence of chiral helical polymers and true PBG can allow for the formation of optically active photonic crystal films with tunable CD signals approaching the PBG by readily regulating the lattice constant of PC film fabricated by different-sized nanoparticles as the template.

Considering that the integration of combining the AIEgens and chiroptical materials into the photonic crystal matrix may give rise to the promotion of chirality transform between the fluorescent units and chiral helical polymer chains, and functional photonic crystal films are inclined to generate remarkable circularly polarized luminescence emissions. As demonstrated in Fig. 4a–e, a pair of mirror-image CPL signals emerge at approximately 500 nm, in which the peak position is located near the PL emission peaks of the TPE monomer with a positive sign for left handedness and a negative sign for right handedness. This indicates that the effective chirality transform occurs under this condition, clearly elucidating the synergistic effect of chiroptical helical polymers, and aggregate-state AIE molecules greatly facilitate the generation of emitting mirror-symmetric CPL responses. However, the generation of CPL performance can be induced from the overlapping area of the chiral ingredient's CD spectra and the fluorescent ingredient's PL spectra, which is called the “matching rule”.<sup>70</sup> As

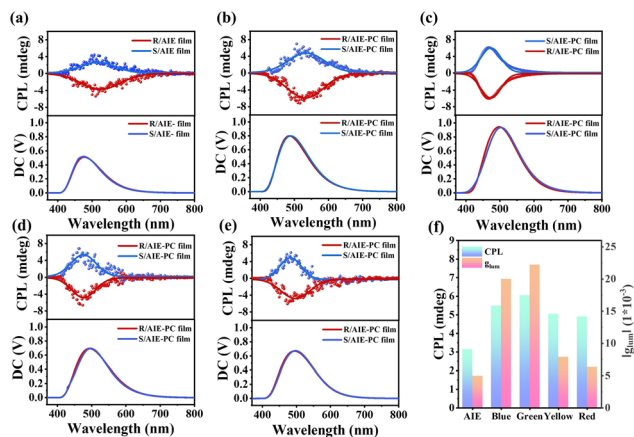


**Fig. 4** Circularly polarized luminescence performance of the composite photonic crystals. CPL spectra of (a) the chiral AIE film and (b) blue, (c) green, (d) yellow and (e) red composite photonic films. (f) CPL intensity and  $|g_{lum}|$  values of the chiral AIE film and various composite photonic films.

shown in Fig. S13,† no CPL signals are observed in the neat PC, AIE or chiral PC films, supporting the absence of chirality transfer and inconsistent with the “matching rule”, which firmly illustrates that the combination of fluorescence and handedness is the essential preconditions for triggering CPL performance. In addition, benefiting from the boosted fluorescent substances, emission propels amplified luminous efficiency for concurrently advancing CPL strength. Fig. 4f depicts the enhanced CPL-active effect in the composite PC films, as evidenced by the obvious increased CPL signal intensity (Fig. 4a–e). This can be explained by the polymerized PC polymer matrix restricting the motions of chiral and fluorescent polymer chains, resulting in multidimensional inter-chain entanglement, which significantly strengthens the RIM effect and chirality fixation, contributing to the enhanced chirality transfer between the bonding luminophores and chiral molecules to enhance the CPL activity.

What is more, the luminescence dissymmetry factor ( $g_{lum}$ ) was employed to evaluate the relative CPL performance of chiral fluorescent PC films.<sup>71,72</sup> As shown in Fig. 4f, the maximum dissymmetry factor in composite films without ordered periodic colloidal arrays ( $|g_{lum}| = 5 \times 10^{-3}$ ) is inferior to that of composite green PC films ( $|g_{lum}| = 22 \times 10^{-3}$ ), which suggests that the incorporation of long-range ordered nanostructure into the chiral fluorescent media could manipulate the dissymmetry of light emission even amplifying CPL response of optically active materials. The boosted CPL and  $|g_{lum}|$  value are mainly attributed to the strengthened PL intensity, that is, the improved efficiency of AIE fluorescence emission is favorable for chirality transfer efficiency and capability. Consequently, integrating chiral fluorescent substances into a photonic crystal matrix encapsulated with a confined rigid polymer network can achieve better chirality fixation and fluorescence enhancement, facilitating strengthened CPL performance in the optically active photonic crystal emitters.



## Conclusion

In summary, we demonstrated the successful fabrication of optically active photonic crystal films based on the integrating system of “AIEgens + chiral helical copolymers”. The enhanced fluorescence properties are obtained from the photonic bandgap edge effect and slow photon effect, which turns out to be the effective induction of radiative pathways by greatly inhibiting the non-radiative decay channel in the confined rigid photonic matrix domains. Interestingly, a pair of emerging mirror-CD signals appear to approach the PBG owing to the band gap separation in the composite photonic crystals composed of chiroptical media. The PL intensity and new CD signal position are highly modulated through precisely tailored PBG of PC by regulating the diameters of colloidal building units. Moreover, the synergistic effect between AIEgens and the chiral helical medium is devoted to the valid chirality transfer to promote emission efficiency, affording the apparent enhanced CPL-active characteristic. This work is envisioned to enrich the foundational comprehension of multi-functional photonic crystals in manipulating light-matter interactions (including AIE luminogens and chirality) for constructing high-performance chirality- or CPL-based optical advanced materials.

## Author contributions

C. Wang and Q. Guo conceived the study and designed the experiments. Q. Guo carried out the experiments under the supervision of J. Guo and C. Wang. X. Huang and H. Li helped with measurements. Q. Guo and C. Wang wrote and revised the manuscript. All authors contributed to this work and have given approval to the final version of the manuscript.

## Data availability

Data are available upon request from the authors.

## Conflicts of interest

The authors declare no competing financial interest.

## Acknowledgements

This work was supported financially by National Natural Science Foundation of China (Grant No. 52131308, 52373131), MOST (2022YFA1203002), and Key Research and Development Project of Guangdong Province (Grant No. 2020B010190003).

## References

- 1 P. Singh, G. Dosovitskiy and Y. Bekenstein, *ACS Nano*, 2024, **18**, 14029–14049.
- 2 R. Xiong, J. Luan, S. Kang, C. Ye, S. Singamaneni and V. V. Tsukruk, *Chem. Soc. Rev.*, 2020, **49**, 983–1031.
- 3 P. Wu, J. Wang and L. Jiang, *Mater. Horiz.*, 2020, **7**, 338–365.
- 4 S. Tadepalli, J. M. Slocik, M. K. Gupta, R. R. Naik and S. Singamaneni, *Chem. Rev.*, 2017, **117**, 12705–12763.
- 5 D. Gur, B. A. Palmer, S. Weiner and L. Addadi, *Adv. Funct. Mater.*, 2017, **27**, 1603514.
- 6 G. England, M. Kolle, P. Kim, M. Khan, P. Muñoz, E. Mazur and J. Aizenberg, *Proc. Natl. Acad. Sci. U. S. A.*, 2014, **111**, 15630–15634.
- 7 S. Vignolini, P. J. Rudall, A. V. Rowland, A. Reed, E. Moyroud, R. B. Faden, J. J. Baumberg, B. J. Glover and U. Steiner, *Proc. Natl. Acad. Sci. U. S. A.*, 2012, **109**, 15712–15715.
- 8 S. Caffarri, K. Broess, R. Croce and H. van Amerongen, *Biophys. J.*, 2011, **100**, 2094–2103.
- 9 V. Saranathan, C. O. Osuji, S. G. J. Mochrie, H. Noh, S. Narayanan, A. Sandy, E. R. Dufresne and R. O. Prum, *Proc. Natl. Acad. Sci. U. S. A.*, 2010, **107**, 11676–11681.
- 10 P. Vukusic and J. R. Sambles, *Nature*, 2003, **424**, 852–855.
- 11 S. Yoshioka and S. Kinoshita, *Proc. R. Soc. London, Ser. B*, 2004, **271**, 581–587.
- 12 P. Vukusic, J. R. Sambles, C. R. Lawrence and R. J. Wootton, *Proc. R. Soc. London, Ser. B*, 1999, **266**, 1403–1411.
- 13 V. Sharma, M. Crne, J. O. Park and M. Srinivasarao, *Science*, 2009, **325**, 449–451.
- 14 X. Zhang, T. Yin and J. Ge, *Adv. Mater.*, 2023, **36**, 2309344.
- 15 J. Fonseca, L. Meng, P. Moronta, I. Imaz, C. López and D. Maspoch, *J. Am. Chem. Soc.*, 2023, **145**, 20163–20168.
- 16 Z. Wang, Y. Wang, Z. Ge, Y. Tian, M. Ai, S. Cao, M. Wang, S. Wang and J. Ma, *Matter*, 2022, **5**, 4060–4075.
- 17 Y. L. Shi, Q. Lv, Y. C. Tao, Y. X. Ma and X. D. Wang, *Angew. Chem., Int. Ed.*, 2022, **61**, e202208768.
- 18 R. Lin, Y. Qi, D. Kou, W. Ma and S. Zhang, *Adv. Funct. Mater.*, 2022, **32**, 2207691.
- 19 Z. Li, X. Wang, L. Han, C. Zhu, H. Xin and Y. Yin, *Adv. Mater.*, 2022, **34**, e2107398.
- 20 J. Zhang, J. Zhang, Y. Ou, Y. Qin, H. Wen, W. Dong, R. Wang, S. Chen and Z. Yu, *Small*, 2021, **17**, e2007426.
- 21 D. P. Song, T. H. Zhao, G. Guidetti, S. Vignolini and R. M. Parker, *ACS Nano*, 2019, **13**, 1764–1771.
- 22 X. Yu, J. Wu, J. Wang, N. Zhang, R. Qing, G. Li, Q. Li and S. Chen, *Adv. Mater.*, 2024, **36**, 2312879.
- 23 J. Wu, X. Yu, G. Li and S. Chen, *Chin. Chem. Lett.*, 2024, **35**, 109234.
- 24 D. Pocięcha, N. Vaupotič, M. Majewska, E. Cruickshank, R. Walker, J. M. D. Storey, C. T. Imrie, C. Wang and E. Gorecka, *Adv. Mater.*, 2021, **33**, 2103288.
- 25 Z. Cai, Z. Li, S. Ravaine, M. He, Y. Song, Y. Yin, H. Zheng, J. Teng and A. Zhang, *Chem. Soc. Rev.*, 2021, **50**, 5898–5951.



- 26 Y. Wang, W. Li, M. Li, S. Zhao, F. De Ferrari, M. Liscidini and F. G. Omenetto, *Adv. Mater.*, 2018, **31**, 1805312.
- 27 E. S. A. Goerlitzer, R. N. Klupp Taylor and N. Vogel, *Adv. Mater.*, 2018, **30**, e1706654.
- 28 Y. Liu and A. A. Houck, *Nat. Phys.*, 2016, **13**, 48–52.
- 29 M. Kuang, J. Wang and L. Jiang, *Chem. Soc. Rev.*, 2016, **45**, 6833–6854.
- 30 E. Yablonovitch, *Phys. Rev. Lett.*, 1987, **58**, 2059–2062.
- 31 S. John, *Phys. Rev. Lett.*, 1987, **58**, 2486–2489.
- 32 L. Ondič, M. Varga, K. Hruška, J. Fait and P. Kapusta, *ACS Nano*, 2017, **11**, 2972–2981.
- 33 J. Liu, H. Zhao, M. Wu, B. Van der Schueren, Y. Li, O. Deparis, J. Ye, G. A. Ozin, T. Hasan and B. L. Su, *Adv. Mater.*, 2017, **29**, 1605349.
- 34 K. Chen, S. Schünemann and H. Tüysüz, *Angew. Chem., Int. Ed.*, 2017, **56**, 6548–6552.
- 35 H. Li, J. Wang, F. Liu, Y. Song and R. Wang, *J. Colloid Interface Sci.*, 2011, **356**, 63–68.
- 36 Y. Zhang, P. Han, H. Zhou, N. Wu, Y. Wei, X. Yao, J. Zhou and Y. Song, *Adv. Funct. Mater.*, 2018, **28**, 1802585.
- 37 J. I. L. Chen, G. von Freymann, S. Y. Choi, V. Kitaev and G. A. Ozin, *J. Mater. Chem.*, 2008, **18**, 369–373.
- 38 Z. Chen, H. Jia, Z. Liu, Y. Chen and J. Wei, *Chem. Eng. J.*, 2024, **480**, 148185.
- 39 S. Liu, Y. Cheng, Y. Li, M. Chen, J. W. Y. Lam and B. Z. Tang, *ACS Nano*, 2020, **14**, 2090–2098.
- 40 V. V. Vipin, P. R. Chandran, A. M. Ramachandran, A. P. Mohamed and S. Pillai, *New J. Chem.*, 2019, **43**, 16264–16272.
- 41 L. Zhang, J. Wang, S. Tao, C. Geng and Q. Yan, *Adv. Opt. Mater.*, 2018, **6**, 1701344.
- 42 Z. Yin, H. Li, W. Xu, S. Cui, D. Zhou, X. Chen, Y. Zhu, G. Qin and H. Song, *Adv. Mater.*, 2016, **28**, 2518–2525.
- 43 S. H. Kim, K.-S. Kim, K. Char, S. I. Yoo and B.-H. Sohn, *Nanoscale*, 2016, **8**, 10823–10831.
- 44 H. Li, J. Wang, H. Lin, L. Xu, W. Xu, R. Wang, Y. Song and D. Zhu, *Adv. Mater.*, 2010, **22**, 1237–1241.
- 45 J. Lv, D. Ding, X. Yang, K. Hou, X. Miao, D. Wang, B. Kou, L. Huang and Z. Tang, *Angew. Chem., Int. Ed.*, 2019, **58**, 7783–7787.
- 46 K. Hou, W. Ali, J. Lv, J. Guo, L. Shi, B. Han, X. Wang and Z. Tang, *J. Am. Chem. Soc.*, 2018, **140**, 16446–16449.
- 47 H. Zhong, B. Zhao and J. Deng, *Adv. Opt. Mater.*, 2023, **11**, 2202787.
- 48 H. Yan, X. Yin, D. Wang, T. Han and B. Z. Tang, *Adv. Sci.*, 2023, **10**, 2305149.
- 49 H. Yan, Y. He, D. Wang, T. Han and B. Z. Tang, *Aggregate*, 2023, **4**, e331.
- 50 X. Yang, J. Lv, J. Zhang, T. Shen, T. Xing, F. Qi, S. Ma, X. Gao, W. Zhang and Z. Tang, *Angew. Chem., Int. Ed.*, 2022, **61**, e202201674.
- 51 X. Gao, B. Zhao and J. Deng, *Macromolecules*, 2022, **55**, 10618–10627.
- 52 N. Lu, X. Gao, M. Pan, B. Zhao and J. Deng, *Macromolecules*, 2020, **53**, 8041–8049.
- 53 M. Khorloo, X. Yu, Y. Cheng, H. Zhang, S. Yu, J. W. Y. Lam, M. Zhu and B. Z. Tang, *ACS Nano*, 2020, **15**, 1397–1406.
- 54 Y. Sang, J. Han, T. Zhao, P. Duan and M. Liu, *Adv. Mater.*, 2019, **32**, 1900110.
- 55 J. Han, D. Yang, X. Jin, Y. Jiang, M. Liu and P. Duan, *Angew. Chem., Int. Ed.*, 2019, **58**, 7013–7019.
- 56 A. K. Srivastava, W. Zhang, J. Schneider, A. L. Rogach, V. G. Chigrinov and H. S. Kwok, *Adv. Mater.*, 2017, **29**, 1701091.
- 57 C. He, G. Yang, Y. Kuai, S. Shan, L. Yang, J. Hu, D. Zhang, Q. Zhang and G. Zou, *Nat. Commun.*, 2018, **9**, 5117.
- 58 J. Han, S. Guo, H. Lu, S. Liu, Q. Zhao and W. Huang, *Adv. Opt. Mater.*, 2018, **6**, 1800538.
- 59 M. D. Turner, M. Saba, Q. Zhang, B. P. Cumming, G. E. Schröder-Turk and M. Gu, *Nat. Photonics*, 2013, **7**, 801–805.
- 60 J.-J. Kim, Y. Lee, H. G. Kim, K.-J. Choi, H.-S. Kweon, S. Park and K.-H. Jeong, *Proc. Natl. Acad. Sci. U. S. A.*, 2012, **109**, 18674–18678.
- 61 X. Du, J. Liu, J. Deng and W. Yang, *Polym. Chem.*, 2010, **1**, 1030–1038.
- 62 Q. Guo, S. Chen, H. Li, X. Wang, J. He, J. Chu, J. Guo and C. Wang, *Chem. Eng. J.*, 2024, **488**, 150969.
- 63 Z. Zhao, H. Zhang, J. W. Y. Lam and B. Z. Tang, *Angew. Chem., Int. Ed.*, 2020, **59**, 9888–9907.
- 64 J. Mei, Y. Hong, J. W. Y. Lam, A. Qin, Y. Tang and B. Z. Tang, *Adv. Mater.*, 2014, **26**, 5429–5479.
- 65 J. Mei, N. L. C. Leung, R. T. K. Kwok, J. W. Y. Lam and B. Z. Tang, *Chem. Rev.*, 2015, **115**, 11718–11940.
- 66 S. Wu, H. Xia, J. Xu, X. Sun and X. Liu, *Adv. Mater.*, 2018, **30**, 1803362.
- 67 D. Li, D. Zhou, W. Xu, X. Chen, G. Pan, X. Zhou, N. Ding and H. Song, *Adv. Funct. Mater.*, 2018, **28**, 1804429.
- 68 C. He, M.-H. Lu, R.-C. Yin, T. Fan and Y.-F. Chen, *J. Appl. Phys.*, 2010, **108**, 073103.
- 69 L. Junqing, J. Lei, L. Li and L. Chunfei, *IEEE Photonics Technol. Lett.*, 2006, **18**, 1261–1263.
- 70 B. Zhao, K. Pan and J. Deng, *Macromolecules*, 2018, **52**, 376–384.
- 71 C. Zhang, S. Li, X. Y. Dong and S. Q. Zang, *Aggregate*, 2021, **2**, c48.
- 72 M. Hu, H.-T. Feng, Y.-X. Yuan, Y.-S. Zheng and B. Z. Tang, *Coord. Chem. Rev.*, 2020, **416**, 213329.

